Astron. Astrophys. 362, 236–244 (2000)

ASTRONOMY AND ASTROPHYSICS

Spectroscopy of the candidate luminous blue variable at the center of the ring nebula G79.29+0.46

R.H.M. Voors[1,2⋆], T.R. Geballe[3], L.B.F.M. Waters[4,5], F. Najarro[6], and H.J.G.L.M. Lamers[1,2]

[1] Astronomical Institute, University of Utrecht, Princetonplein 5, 3508 TA Utrecht, The Netherlands
[2] SRON Laboratory for Space Research, Sorbonnelaan 2, 3584 CA Utrecht, The Netherlands
[3] Gemini Observatory, 670 N. A'ohoku Place, Hilo, Hawaii 96720, USA
[4] Astronomical Institute 'Anton Pannekoek', University of Amsterdam, Kruislaan 403, 1098 SJ Amsterdam, The Netherlands
[5] SRON Laboratory for Space Research, P.O. Box 800, 9700 AV Groningen, The Netherlands
[6] CSIC Instituto de Estructura de la Materia, Dpto. Fisica Molecular, C/Serrano 121, 28006 Madrid, Spain

Received 23 March 2000 / Accepted 14 July 2000

Abstract. We report optical and near-infrared spectra of the central star of the radio source G79.29+0.46, a candidate luminous blue variable. The spectra contain numerous narrow (FWHM $< 100\,\mathrm{km\,s^{-1}}$) emission lines of which the low-lying hydrogen lines are the strongest, and resemble spectra of other LBVc's and B[e] supergiants. A few prominent infrared lines are unidentified. The terminal wind speed is determined from Hα to be $110\,\mathrm{km\,s^{-1}}$. The strength of Hα implies the presence of a very dense wind. Extended emission from Hα and [N II] was detected but appears to be associated with the Cygnus X region rather than the radio source. Both diffuse interstellar bands and interstellar absorption lines are present in the optical spectrum of the central star, suggesting that there are both diffuse and molecular cloud components to the extinction and implying a minimum distance of 1 kpc and minimum luminosity of $\sim 10^5\,\mathrm{L_\odot}$ for the star. The new spectra and their analysis indicate a low excitation, dense, and slowly expanding wind and support the LBVc classification.

Key words: stars: circumstellar matter – stars: early-type – stars: evolution – stars: individual: G79.29+0.46 – stars: mass-loss – stars: variables: general

1. Introduction

Many gaps exist in the understanding of the post-main sequence evolution of the most massive ($> 40\,\mathrm{M_\odot}$) stars, due in large part to the small number of such stars identified as being in this evolutionary phase. It is known that during part of the post-main sequence phase, identified as the Luminous Blue Variable (LBV) stage (Conti 1984), these stars lose a large amount of mass in a short time interval (e.g. Chiosi & Maeder 1986). The identifying characteristics of an LBV in addition to its blue colors are (1) a mass loss rate of ($\sim 10^{-5}\,\mathrm{M_\odot\,yr^{-1}}$), (2) a low wind velocity of no more than a few hundred $\mathrm{km\,s^{-1}}$, (3) photometric variations of up to 2 magnitudes on time-scales ranging from months to decades, and (4) the presence of a circumstellar (and sometimes bipolar) nebula (Nota & Clampin 1997).

Less than a dozen confirmed LBVs are known in our Galaxy. However, in recent years a number of LBV candidates (LBVc's) have been found. Candidates generally have both of the first two characteristics listed above and one of the other two (for reviews see Nota & Lamers 1997). One recently discovered LBVc is the central star of the radio shell G79.29+0.46 (Higgs et al. 1994, hereafter HWL; and Waters et al. 1996, hereafter Paper I). The principal evidence for its candidacy are its high luminosity and mass loss rate (estimated as $\sim 1 \times 10^{-6}\,\mathrm{M_\odot\,yr^{-1}}$ in Paper I) and the presence of a slightly bipolar ring nebula. Few spectra have been reported and the only spectral features in them thought to be associated with the star are several recombination lines of hydrogen and helium, most notably Hα (HWL) and Brα (Paper I). HWL also reported the presence of diffuse interstellar lines and bands.

In this paper we present and discuss additional optical and near-infrared spectra of the central star of G79.29+0.46 (hereafter G79*). The resolution of the optical spectrum is considerably higher than the spectrum published by HWL and the infrared spectra provide considerably more wavelength coverage than the spectrum in Paper I. The new spectra allow us to estimate the excitation, luminosity and current activity of the star. We conclude that although G79* may have gone through a more intense mass loss episode in the recent past, it probably still is in the luminous blue variable stage of evolution.

2. Observations and data reduction

2.1. Optical

A log of observations is provided in Table 1. High resolution optical spectra of G79* were obtained in 1995 with the Utrecht Echelle Spectrograph (UES) mounted on the William Herschel Telescope on La Palma. The TEK 5 detector (1024×1024 pix-

Send offprint requests to: L.B.F.M. Waters (rensw@astro.uva.nl)

⋆ *Present address:* KNMI (Royal Dutch Meteorological Institute), Sectie Astmospherische Samenstelling, Postbus 201, 3730 AE De Bilt, The Netherlands

Table 1. Observing log

Date	Resolving Power	Range (μm)
1995 Aug 3	44,000	0.54–0.76
1995 Aug 3	44,000	0.54–0.90
1996 Jul 15	2515–2775	1.07–1.18
1996 Jul 16	2540–2800	1.62–1.78
1996 Jul 17	1600–1870	2.05–2.38
1997 May 8	800–1050	1.01–1.34
1997 May 8	725–1000	1.86–2.52

els) was used. The slit length was 15 arcsec, allowing a portion of the nebula to be observed simultaneously. Insufficient time was available to obtain the blue part of the spectrum, which is very faint due to the high extinction. Two overlapping settings were chosen to cover the red part of the spectrum, with three exposures obtained at each setting. A spectrum of a ThAr lamp combined with telluric lines in the spectrum of the G79* allowed the wavelength calibration to be determined to an accuracy of 1 km s^{-1} and provided an estimate of $\sim 44,000$ for the resolving power.

Data reduction used the Midas echelle package. Because of the faintness of the object ($V \approx 16$ mag is about the limiting magnitude for the UES) and because the position of the orders on the CCD was not constant during the night, considerable care had to be taken (for details see Voors 1999). The signal-to-noise ratio of the continuum in the final spectrum (not shown) increases from ≈ 5 around 6000 Å to ≈ 50 around 8000 Å.

2.2. Infrared

Spectra covering portions of the 1.0–2.5 μm band were obtained at the 3.8m United Kingdom Infrared Telescope (UKIRT) on Mauna Kea in 1996 and 1997. The facility cold grating spectrometer CGS4 (Mountain et al. 1990) was used for all observations, with its 80″ slit of width of 1.″2 oriented east-west. In 1996 a 150 l/mm grating was used, providing a relatively narrow wavelength coverage and high spectral resolution; in 1997 a 75 l/mm grating was employed to provide wider spectral coverage at lower resolution. The resolving powers, $\lambda/\Delta\lambda$, given in Table 1 increase with wavelength in each spectral interval and are those of the original (unreduced) spectra. Observations were made in the standard stare/nod-along-slit mode, with a nod of $\approx 15''$; thus any constant extended emission (from the nebula or background) along the slit was subtracted away.

The spectra were wavelength-calibrated using observations of Kr and Ar arc lamps made nearly simultaneously with the measurements of G79*, were flux-calibrated and corrected for telluric absorption features using observations of nearby bright dwarf stars with spectral types from mid to late F, and then were slightly smoothed (reducing the resolving powers by 20% from those given in Table 1). Brackett and Paschen series absorption lines in clear parts of the spectrum were edited out of the dwarf star spectra prior to ratioing; the uncertainties in this procedure lead to significant uncertainties in the strengths of the weak Brackett series lines in G79* in the H band and to slight uncertainty in the details of the wings of its Brγ line. The noise level at most wavelengths can be estimated from the (small) fluctuations in flat portions of the spectrum. Near 1.9 μm, strong telluric water vapor absorption is responsible for large systematic fluctuations. The rms wavelength accuracy is typically $\pm$0.0002 μm.

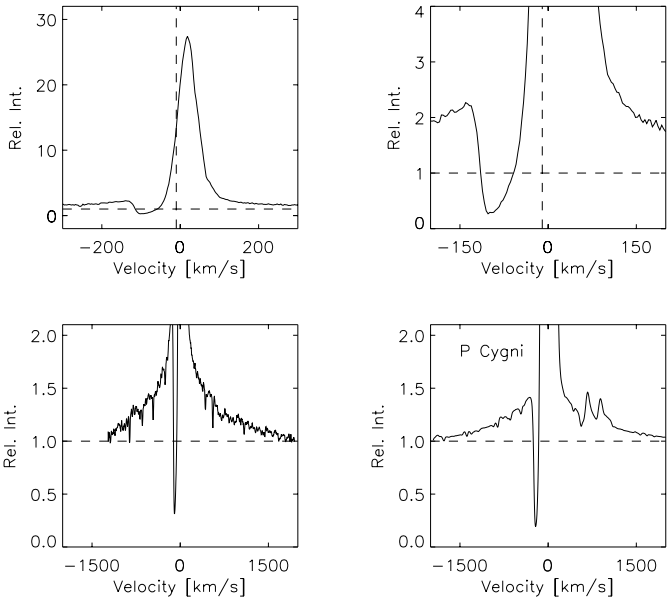

Fig. 1. The Hα line profile in G79*, shown in three different velocity and intensity scales, and in P Cygni (bottom right)

The J band spectrum obtained in 1996 with the 150 l/mm grating in third order was contaminated shortward of 1.105 μm by continuum emission near 1.6 μm in second order; this was corrected assuming no strong emission lines were present near 1.6 μm and that the slope of the J band continuum longward of 1.105 μm extrapolated shortward of 1.105 μm. These assumptions are borne out by the uncontaminated spectrum obtained in 1997 with the 75 l/mm grating in second order.

3. The spectrum of the star and its wind

3.1. Optical

The optical spectrum of G79* contains a number of lines originating in the stellar photosphere and wind, extended line emission from [N II] and Hα, and diffuse interstellar bands (DIBs). Table 2 lists the identified stellar lines, their measured central wavelengths, type of profile, and total equivalent width. Figs. 1–4 show many of these lines. Both pure emission and absorption profiles are observed as well as hybrids. Some of these lines appear to be formed entirely in the wind, whereas others show photospheric contributions. Because of their wind origins, the hydrogen and helium lines are unsuitable for determination of the radial velocity of the star. Instead we use the weak emission lines of metals, whose profiles appear similar (e.g., Fig. 3) to derive V_{hel} = -10 $\pm$ 2 km s^{-1} (corresponding to V_{LSR} = -

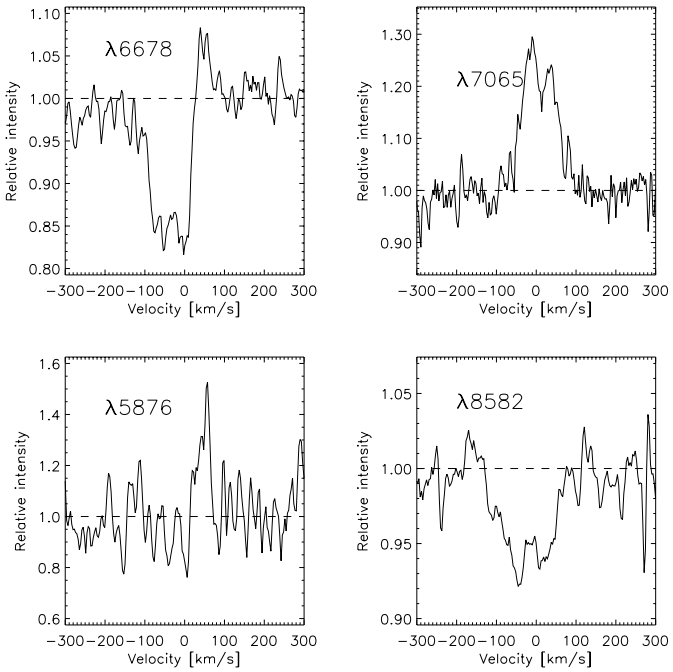

Fig. 2. Profiles of four He I lines in G79*.

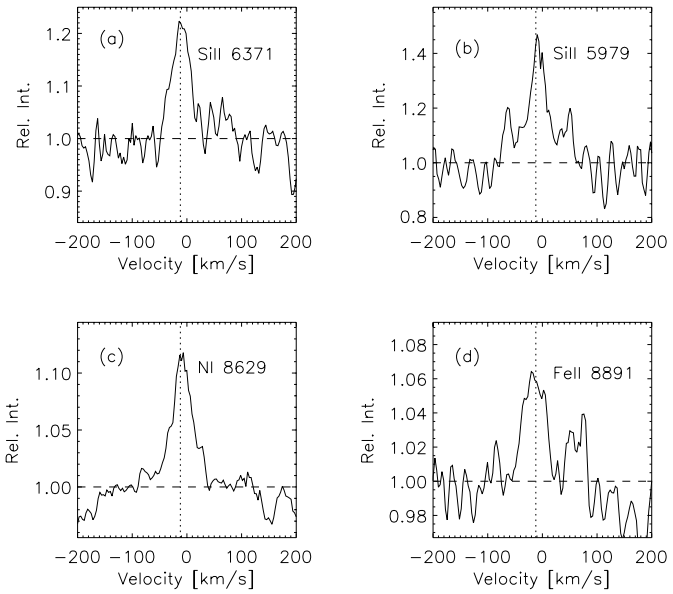

Fig. 3a–d. Representative metallic lines in G79*. The dashed vertical line corresponds to the derived stellar radial velocity of -10 km s^{-1} (hel.).

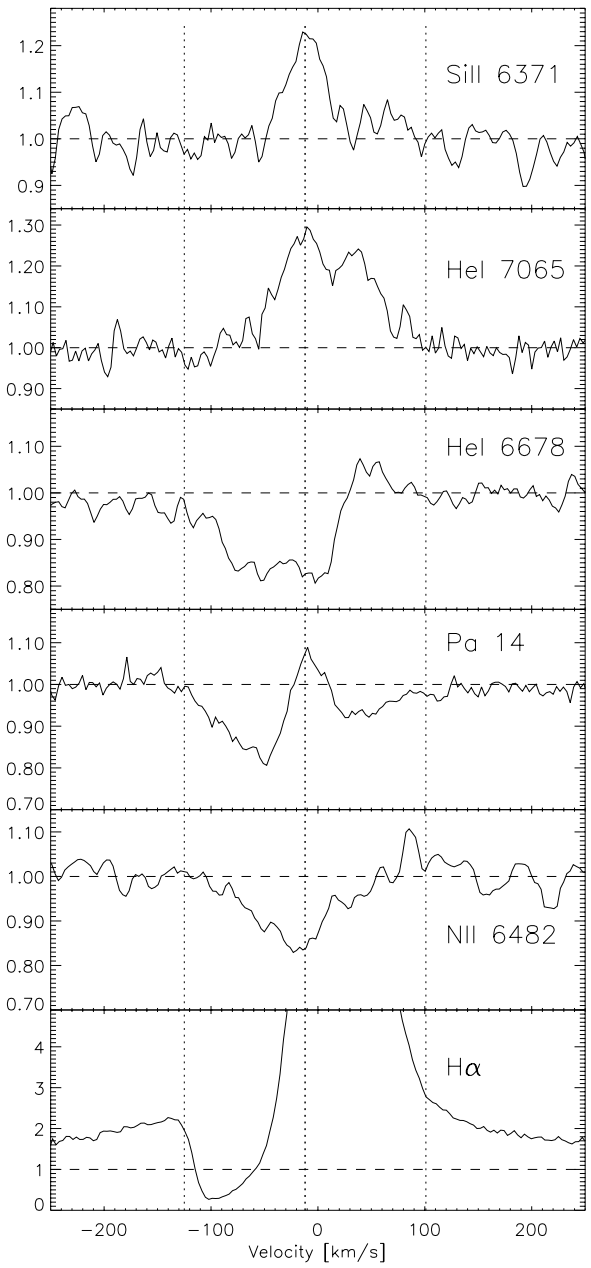

Fig. 4. Representative line profiles in G79*. The dashed vertical lines correspond to the derived radial velocity of -10 km s^{-1} (hel.) and wind speed of 110 km s^{-1}.

27 km s^{-1}), a result intermediate between those of HWL and Paper I.

3.1.1. Hydrogen lines

The Hα line (Fig. 1), which dominates the optical spectrum, has a strong central emission peak, a blueshifted absorption component, and broad and shallow wings. Contributions by nebular emission to each of these are negligible. The overall profile is similar to that seen in other luminous blue supergiants. In P Cygni the broad and shallow wings to Hα are believed to be caused by the scattering of photons by electrons (Münch 1948, Bernat & Lambert 1978). We make the same interpretation for G79*, as suggested in Paper I, concurring that the wind velocity of 1400 km s^{-1} derived by HWL is erroneous. The wings in G79* and P Cygni are approximately the same width, but those in G79* are about twice as strong. Scattering wings are not evident in the Brα profile in Paper I.

Despite the strong similarity of the Hα profiles in G79* and P Cygni, direct comparison of the profiles does not give a use-

Table 2. Optical lines

λ_{cen} [Å][1]	λ_{lab} [Å][1]	[Elem.]	Trans. + multiplet	Type[2]	EW [Å][3]
6563.1	6562.797	H I	2-3 (Hα) (1)	pc	51
8598.1	8598.396	H I	3-15 (Pa 14) (9)	ph + pc	-0.40
8545.0	8545.387	H I	3-14 (Pa 15) (10)	ph + pc	
8582.1	8582.670	He I	3p3P - 10d3D	ph	-0.28
	8581.856	He I	3d3D - 14f3F	ph	
6679.1	6678.154	He I	2p1P - 3d1D (46)	ph + pc	-0.41
7065.2	7065.176	He I	2p3P - 3s3S (10)	em	0.56
6577.9	6578.052	C II	3s2S - 3p2P (2)	abs	(-0.2)
6582.6	6582.882	C II	3s2S - 3p2P (2)	abs	(-0.1)
7231.0	7231.333	C II	3p2P - 3d2D (3)	em	(0.1)
7236.1	7236.420	C II	3p2P - 3d2D (3)	em	
8628.9	8629.235	N I	3s2P - 3p2P (8)	em	0.12
	8594.000	N I	3s2P - 3p2P (8)	em	
7423.2	7423.641	N I	3s4P - 3p4S (3)	em	
7441.9	7442.298	N I	3s4P - 3p4S (3)	em	0.02
7468.1	7468.312	N I	3s4P - 3p4S (3)	em	(0.05)
6481.6	6482.048	N II	3s1P - 3p1P (8)	abs	-0.23
5675.7	5676.017	N II	3s3P - 3p3D (3)	abs	
5679.4	5679.558	N II	3s3P - 3p3D (3)	abs	-0.20:
5686.0	5686.213	N II	3s3P - 3p3D (3)	abs	-0.17
6402.1	6402.246	Ne I	3s1 - 3p1 (1)	abs	-0.10
8234.3	8234.636	Mg II	4p2P - 5s2S (7)	em	
7056.4	7056.712	Al II	s4s3S - s4p*3P (3)	em	0.14
7471.1	7471.410	Al II	s3d1D - s4f*1F (21)	em	0.04
6836.8	6837.128	Al II	s4p*3P - s5s3S (9)	em	0.02
6231.5	6231.750	Al II	s4p*3P - s4d3D (10)	em	0.19
6226.0	6226.195	Al II	s4p*3P - s4d3D (10)	em	(0.1)
5957.3	5957.559	Si II	4p2P - 5s2S (4)	em	(0.1)
5978.7	5978.930	Si II	4p2P - 5s2S (4)	em	0.36:
6371.0	6371.371	Si II	4s2S - 4p2P (2)	em	0.21
7462.1	7462.654	Si III	s4d3D - s5p*3P	em	0.07
7466.0	7466.321	Si III	s4d3D - s5p*3P	em	(0.05)
7512.9	7513.162	Fe II	(5D)5s e6D - (5D)5p w6P	em	0.06
7731.3	7731.673	Fe II	(5D)5s e6D - (5D)5p w6P	em	0.05:
8890.6	8890.899	Fe II	(3F2)4p y4F - 4s2 4F	em	0.11
8897.8	8897.810	Fe II	(3F2)4p y4F - 4s2 4F	em	0.06
8926.4	8926.635	Fe II	(5D)5s e4D - (5D)5p 4D	em	0.09:

[1] In air

[2] pc = P Cygni; em = emission line; abs = absorption line (in stellar wind); ph = photospheric

[3] Colons denotes uncertainties of 20-50 percent; values in parentheses are marginal detections, uncertain by at least 50 percent; no value indicates contamination by telluric absorption; all other uncertainties are less than 20 percent.

ful estimate of the mass loss rate from G79*. The strength of scattering wings depends on the relative strengths of the line and continuum radiation fields and the electron scattering optical depth in the region where the line forms. These in turn are determined by the rate of mass loss, the velocity field, and the effective temperature of the star. The uncertainty in the distance to G79* (1 to 4kpc, see below) implies a factor of 8 uncertainty in the mass loss rate. This uncertainty is further increased if the two stars have different velocity fields. Moreover, even if the same radius and velocity structure are assumed for both objects a direct comparison would still fail due to the remarkably different ionizations of P Cygni and G79*. The weakness of the He I lines as well as the presence of N I and O I lines in the G79* spectrum denote a lower effective temperature for this object than P Cygni. A difference in the effective temperature is translated not only into a difference in the radiation field in the line (which affect the electron scattering wings), but also into a difference in the run of the departure coefficients which control the overall line emission. Although the strength of Hα in G79* indicates the presence of a very dense stellar wind, an accurate estimate of the mass loss rate can be achieved only through detailed quantitative analysis.

Although the Hα line profile is unsuitable for determining the stellar radial velocity, the blueshifted absorption feature allows an accurate determination of the terminal wind speed (Fig. 4). The short wavelength edge of this absorption occurs at

V_{hel} = -120 km s^{-1}, implying a wind speed of 110 km s^{-1} (if turbulence in the wind is small). This compares with the value of 94 km s^{-1} obtained in Paper I based on the FWZI of the lower signal-to-noise ratio Brα line profile, which has only a weak blueshifted absorption feature. On the positive velocity side of the profile, a change in slope is evident at V_{hel} = +100 km s^{-1}, beyond which the scattering wing dominates, in good agreement with the newly derived wind speed.

The Pa 14 profile, which also is shown in Fig. 4, is considerably different from Hα. The emission component, seen near line center is formed in the wind, where non-LTE effects tend to overpopulate the high levels. The absorption wings are formed in the photosphere.

3.1.2. Helium lines

Four helium lines were detected in the UES spectrum and are shown in Fig. 2. The He I 7065 profile shows two peaks, centered at -12 km s^{-1} and $+37$ km s^{-1} (hel.). The profile shown is corrected for telluric H_2O lines, and the dip near $v = +10$ km s^{-1} is real. The blue peak at -12 km s^{-1} coincides with the system velocity, suggesting that it is formed near the star, where the outflow velocity is low. If the second peak at +37 km s^{-1} is formed in a rotating disk, in matter ejected by the star, or in a companion star, it is not clear why this feature would not be present in lines of other elements. In contrast, the He I 6678 line has a P Cygni profile. Assuming G79* to be spherically symmetric, the presence of some absorption redshifted from the stellar velocity of -10 km s^{-1} indicates a substantial photospheric contribution. However, it is not clear why He I 6678, which has a larger oscillator strength than He I 7065 shows the larger photospheric contribution.

The He I 5876 line peak occurs at $+40$ km s^{-1}, coinciding with one of the two peaks seen in the λ 7065 and λ 6678 profiles. However, the stronger component at -12 km s^{-1} is not seen. In summary, the helium lines in G79* show large differences from one another, most likely due to non-LTE effects and optical depth effects in the photosphere and wind, but we do not have detailed explanations for their specific disparate behaviors.

3.1.3. Metal lines

Among the metallic lines in the optical spectrum of G79* the N II lines, the C II lines and the Ne I 6402 line are in absorption; all others are in emission. A number of emission line profiles are shown in Fig. 3; these and others have been used to estimate the radial velocity of G79*, as discussed previously. Those of metals have FWHMs of approximately 50 km s^{-1} and FWZIs of 90 to 100 km s^{-1}. The excitations of the metal lines are low and are typical for mid to late-B type supergiants.

3.2. Infrared

The J and the K band spectra of G79* are shown in Fig. 5, with identifications and equivalent widths given in Tables 3 and 4. Most of the strong lines are standard recombination lines of hydrogen and helium, but there are a few unidentified lines of surprising strength. Where a line was observed more than once, the variation in its equivalent width was less than 10 percent. Furthermore, after convolving the 1996 spectra to the resolution of the 1997 spectra, no significant differences in line shape or width were found.

3.2.1. Identified lines

Several of the prominent infrared lines have profiles worthy of note. The He I 1.083 and 2.058 μm lines possess broad wings, which extend approximately 1,000 km s^{-1} to either side of line center. The wings are somewhat broader in the 1.083 μm line profile. As in the case of Hα, these wings are the result of electron scattering. The weak absorption feature just shortward of Brγ (2.166 μm) is due to absorption by He I 7–4, whose strongest transitions are at 2.165 μm and 2.161 μm (e.g., see Najarro et al. 1994). The equivalent width of this absorption is consistent with the much stronger He I 4-3 absorption at 2.112 μm. The O I line at 1.128 μm displays a long wavelength shoulder, but this may be due to blending with lines of Si III.

Prominent in the K band are two Mg II lines near 2.14 μm. This pair is excited by UV fluorescence. Whether this is continuum or Ly β fluorescence (Bowen 1947) cannot be determined from the present data. The Na I emission lines at 2.206 μm and 2.209 μm also may be excited by fluorescence (Thompson & Boroson 1977) via 3303 Å (continuum) photons. Both the Mg and Na doublets are present in the spectra of LBV and B[e] stars (McGregor et al. 1988). In G79* and Wra 751 the Mg II lines are much stronger than the Na I lines; however, in AG Car the doublets are similar in strength (Morris et al. 1996).

The J band lines of O I at 1.129 μm and 1.317 μm form a third diagnostic infrared pair. The 1.129 μm line is pumped by Ly β, and is only strong relative to the 1.317 μm line if Lyman fluorescence is the dominant source of excitation (Grandi et al. 1975). In G79* this ratio is 8.8 $\pm$ 0.8, implying a strong Ly β flux, as expected.

Pfund series lines are detected in G79* from n=18 to n=37. Observations of higher n lines are made difficult by blending and by the presence of an unidentified line at 2.317 μm. High Pfund series lines also are found in Be stars (e.g. γ Cas; Hamann & Simon 1987).

3.2.2. Unidentified Lines

A number of unidentified infrared lines are observed in G79* and listed in Table 4. The most prominent of these are at 1.0916 and 1.0953 μm. To our knowledge, neither has been seen previously in any other objects. A possible identification for the 1.0916 μm line is the He I 3D-3Fo transition. Also possible are two Mg II 2D-2Po transitions, but they have much lower $\log gf$ values than lines of the same element not seen in the spectrum. A forbidden [Fe II] transition at 1.0957 μm is shifted slightly too far from the 1.0953 μm line to be a serious possibility; moreover a second [Fe II] line at 1.1068 μm would be present. The line at 1.2769 μm, just on the blue side of Pa β, is possibly due

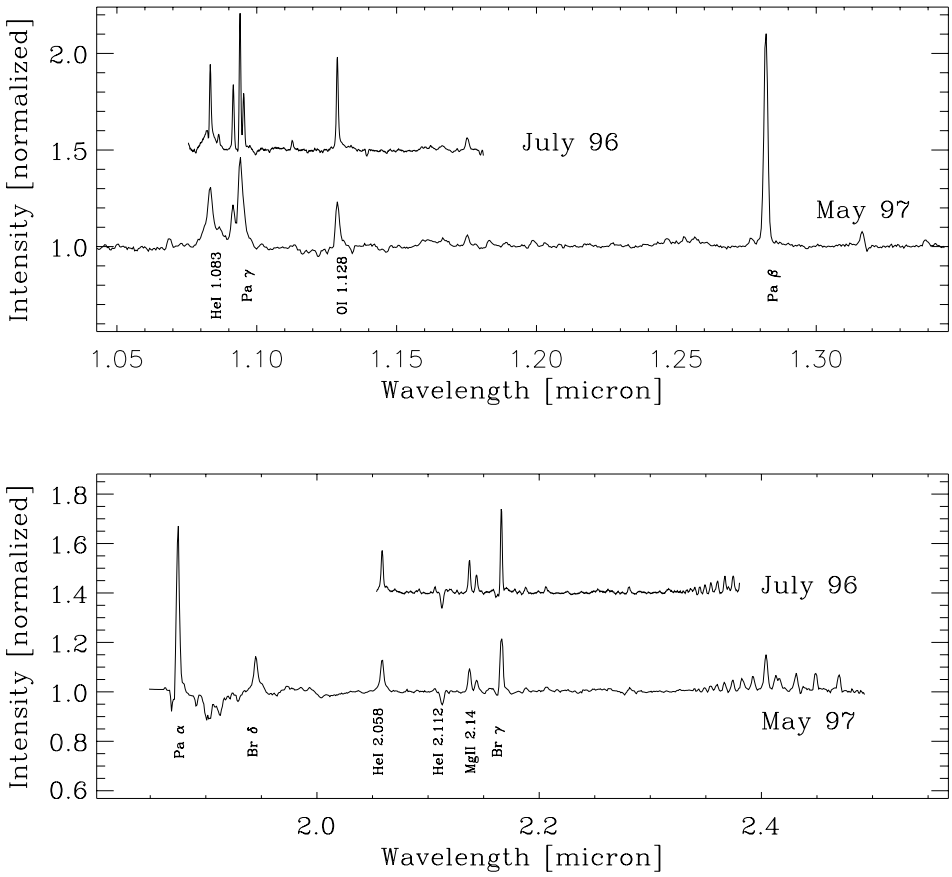

Fig. 5. Infrared spectra of G79*.

to [Fe II]. However, the 1.3098 μm line of the same multiplet should also be present, but is not observed.

3.3. Comparison of G79 with massive supergiants*

The optical–infrared spectrum of G79* most closely resembles those of mid to late type B supergiants. The excitation of the metal lines is typical of such stars. Note, however, that few B-type supergiants have N I emission lines in their optical spectra. Those that do, e.g. HD 326823 (early B), CPD $-52°9243$ (B3), HD 316285 (P Cygni type) (Lopes et al. 1992), are classified as B[e] supergiants. The existences of disks in these sources are inferred from double-peaked line profiles (e.g. HD 326823) or from thermal dust emission (e.g. CPD $-52°9243$). Clearly G79* cannot be such a star, as not only are no forbidden lines detected in its optical spectrum, but also virtually all of its lines lack double-peaked profiles. The narrow hydrogen emission lines seen by us and in Paper I imply massive low velocity winds, similar to those seen in LBVs. This, plus the presence of a circumstellar, dusty nebula suggest that the star is indeed an LBV, even if it is currently not variable.

In Fig. 6 the K band spectra of G79* and three massive supergiants, SGR 1806−20 (van Kerkwijk et al. 1995), Wra 751 and AG Car (Morris et al. 1996), are compared. Wra 751 and AG Car are well studied LBVs. The K band spectrum of SGR 1806−20 is thought to be dominated by a B supergiant whose optical position is close to that of the soft gamma repeater source; note that there is some doubt as to the physical association between the gamma ray source and the B supergiant (Fuchs et al. 1999). The similarity between the spectra of G79* and this star is striking, the main difference being the strength of the (permitted) Fe II 2.089 μm line. As noted by Morris et al. (1996), the near-infrared spectra of many types of massive

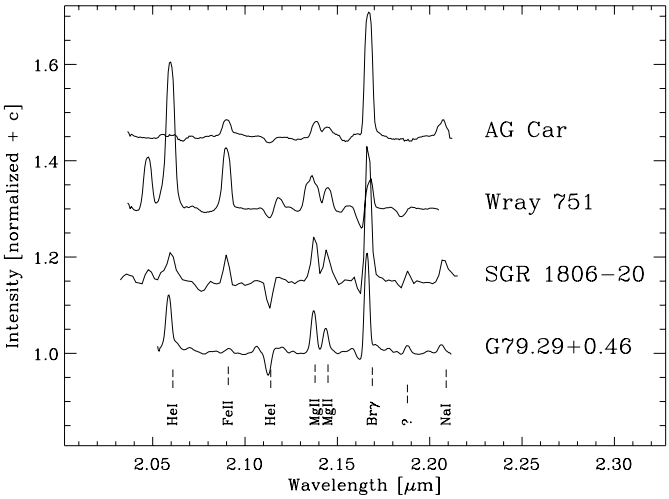

Fig. 6. Comparison of K-band spectra of G79*, the LBVs Wra 751 and AG Car, and the SGR 1806-20, which is dominated by the B supergiant companion.

Table 3. Identified infrared lines

λ_c^{96} [Å][1]	λ_c^{97} [Å][1]	λ_{lab} [Å][1]	Transition	EW [Å][2]
	10687.5	10688.1	C I	0.8
10833.7	10832.9	10833.0	He I	3.2
10863.8	10866	10862.6	Fe II	0.3
10940.1	10940.7	10941.1	Pa γ	4.8
11127.3		11125.6	Fe II	0.4
11288.0	11288.3	11289.4	O I	3.9
11663	11665	11664.1	C I	0.5
11752.5	11752.0	11752.7	C I	0.8
	11830	11831	[Fe II]	0.7
	12466.1	12466.2	N I	0.5
	12566.5	12567.0	[Fe II]	0.5
	12820.1	12821.6	Pa β	19.3
	13164.1	13164.6	O I	1.3
16400		16411.7	Br 12	-
16438.9		16440.0	[Fe II]	-
16875		1.68	Fe II	0.3
16800		16811.1	Br 11	-
16978.5		16976.1	Fe II	$<$0.2
17007.1		17007.0	He I	0.4
17109.3		17115.9	[Fe II]	0.5
17370		17366.6	Br 10	-
17455.7		17454.1	[Fe II]	1.3
	18748.9	18756.1	Paα	-
	19450.5	19450.9	Brδ	5.9
20587.0	20586.5	20586.9	He I	4.4
21125.2	21127.6	21125.8	He I	$-$1.6; blend
		21139.0	He I	blend
21372.6	21373.3	21374.8	Mg II	3.0
21436.4	21436.8	21438.0	Mg II	1.7
21609.9		21613.7	He I	-0.7
21659.7	21662.3	21661.2	Br γ	7.4
22061.4	22067.2	22062.4	Na I	0.7
22081.9		22089.7	Na I	0.2
23191.1		23195.6	Pf 38	$<$0.2
23217.1		23218.0	Pf 37	$<$0.2
23242.1		23242.4	Pf 36	$<$0.2
23268.0		23268.9	Pf 35	$<$0.2
23295.1		23297.9	Pf 34	$<$0.2
23327		23329.6	Pf 33	0.2
23361.8		23364.4	Pf 32	0.3
23400.3	23396.1	23402.8	Pf 31	0.5
23445.3	23433.8	23445.3	Pf 30	0.5
23492.3	23487.5	23492.4	Pf 29	0.7
23545.6	23543.4	23544.8	Pf 28	0.9
23604.5	23599.2	23603.5	Pf 27	1.2
23670.6	23667.4	23669.4	Pf 26	1.4
23746.7	23742.0	23743.8	Pf 25	1.6
	23829.8	23828.2	Pf 24	2.2
	23925.0	23924.7	Pf 23	2.5
		24035.5	Pf 22	blend
	24041.2	24041.5	Mg II	blend
		24044.5	Mg II	5.8; blend
	24131.7	24124.6	Mg II	3.0
	24159.7	24163.9	Pf 21	2.7
	24312.0	24313.6	Pf 20	2.9
	24488.1	24490.0	Pf 19	2.8
	24696.7	24952.5	Pf 18	$\approx$2.5

[1] In vacuo

[2] EW's of H band hydrogen lines highly uncertain and not given.

Table 4. Unidentified infrared lines

λ_c^{96} [Å][1]	λ_c^{97} [Å][1]	EW [Å]	Remarks
10916.0	10915.8	2.5	He I + Mg II?
10953.3		2.3	
	12768.7	1.1	He I?
	13391	0.7	
21062.0	21061.3	0.5	Fe II??
21879.3	21882.0	0.6	Fe II??
22808.4		0.5	N II??
23163.2		0.5	also in AG Car and Wra 751
23703.7		0.6	

[1] In vacuo

evolved stars, are similar; thus one cannot conclude based on their similarity that G79* and the B supergiant in SGR 1806-20 are similar objects.

4. DIBs, interstellar reddening, and luminosity

Table 5 lists the diffuse interstellar absorption bands present in the spectrum of G79*. By comparing the colors of G79* with those of Kurucz (1979) models, HWL derived A_V = 16 mag. We use a different technique, adopting the extinction law for the Cygnus OB2 association (Torres-Dodgen et al. 1991), since that region is probably most representative of the interstellar medium towards G79.29+0.46. Dereddening the JHK spectra as well as the optical spectra published by HWL, and assuming a blackbody temperature for G79* of 18,000 K, results in a derived $E(B-V)$ of 4.9 $\pm$ 0.4. With an R_V of 3.04 this gives an A_V of 14.9 $\pm$ 1.2, which is slightly less than HWL. A lower blackbody temperature for the star, which may be more realistic, would result in a lower derived extinction. In a recent study of the infrared properties of G79.29+0.46 and its star Trams et al. (1999) have derived an $E(B-V)$ of 3.9, corresponding to A_V = 11.9 mag.

The strength of the DIBs are a good measure of the interstellar extinction due to diffuse matter. In several OB associations in Cygnus a tight relation exists between the strength of the λ5797 DIB and $E(B-V)$, (Chlewicki et al., 1986). Assuming this relation for G79.29+0.46, which is very close in the sky to Cyg OB2, we obtain $E(B-V)$ = 2.1 $\pm$ 0.3. This is much less than the values derived above. The discrepancy may be resolved if additional reddening is present in the form of molecular clouds. G79.29+0.46 is only 9′ distant from the center of the obscured star-forming region DR 15, which is thought to contain a few hot stars (Odenwald et al., 1990). An IR spectrum obtained with ISO-SWS Morris et al. (in preparation) shows bands of H_2O and CO_2 ice. It remains to be determined whether the extinction derived from the ISO spectrum accounts for the difference between the two values of $E(B-V)$, but it seems safe to conclude that the extinction to G79.29+0.46 contains both diffuse and molecular contributions.

From the radial velocity of G79* and after allowing for peculiar motions of up to 10 km s^{-1}, we derive a kinematic distance of 2 kpc from the galactic rotation curve with an uncertainty of

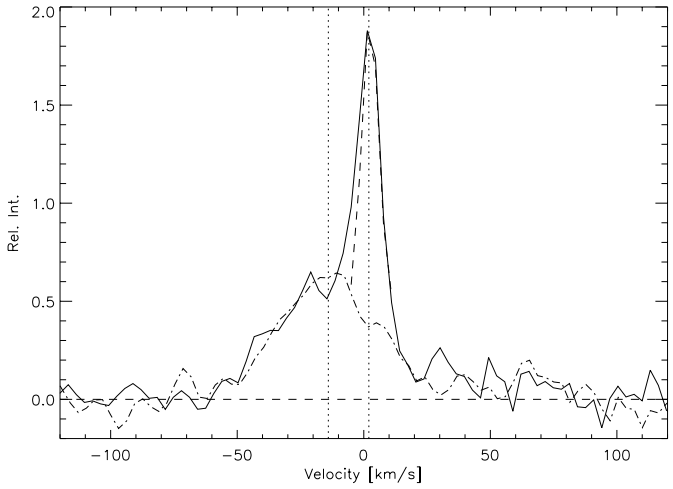

Fig. 7. Average nebular profiles of Hα (solid line) and [N II]λ6583 (dash-dotted line), the latter multiplied by a factor of 2.3. The vertical dotted lines denote the centers of the [N II] line and narrow Hα peak. The dashed line overplotted on Hα peak indicates the spectral resolution.

Table 5. Diffuse interstellar bands

λ_c [Å]	EW [mÅ]	Remarks
8621	585 ± 50	
7927	-	broad feature
7721	60 ± 20	
7585	< 30	
7581	< 30	
7561	85 ± 35	
7559	40 ± 20	
7432	-	broad feature
7334	-	tell. contamination
6993	-	tell. contamination
6940	-	broad feature
6661	41 ± 10	
6379	150 ± 15	
6284	1500 ± 150	
6281	400 ± 100	
6270	150 ± 30	
6204	300 ± 100	
6196	200 ± 70	
5797	260 ± 40	

approximately a factor of two (see, e.g., HWL Fig. 14). Trams et al. use their best fitting model atmosphere, with a luminosity of 3×10^5 L$_\odot$ and mass loss rate of 1.3×10^{-5} M$_\odot$ (considerably higher than the estimate of Paper I) to derive a distance of 1.8 kpc. It is virtually certain that the distance exceeds 0.7 kpc since no interstellar clouds closer than that distance are known which could cause the large observed extinction. The DR 15 complex, which we have suggested is responsible for some of the extinction to G79.29+0.46, is 1 kpc distant. We conclude that the distance to G79.29+0.46 is in the range 1–4 kpc, with a most likely value of $\sim$2 kpc.

5. Extended line emission

Line profiles, averaged along the 15″ slit, excluding the regions influenced by stellar radiation, are shown in Fig. 7. The profile of Hα was averaged over a slightly smaller region along the slit than [N II] λ6583, because of contamination by the bright central peak of stellar Hα. The widths and the shapes of the broad components of the [N II] and the Hα nebular profiles agree very well, Hα being 2.3 times stronger. However, the narrow nebular component seen in Hα is missing in [N II]. Clearly the narrow and broad components originate from different regions.

The broad profiles of both lines are well fitted by a gaussian with FWHM 45 ± 3 km s^{-1}. The FWZI is about 70 km s^{-1}. The central wavelength of the gaussian is $-14\pm$ 2 km s^{-1} and agrees very well with the radial velocity of the central star, -10 km s^{-1}. More recent observations (Voors 1999) show that both the broad and narrow components extend well beyond the ring nebula, implying that they are interstellar in origin and probably associated with emission from the Cygnus-X region.

6. Conclusion: the nature of G79*

Even at the minimum distance of 1 kpc the luminosity of G79* is 1×10^5 L$_\odot$; at the maximum distance of 4 kpc it approaches that of some of the most luminous stars known. Its temperature and spectral type are not well defined, but the presence of neutral species in emission and absorption as well as N II lines in absorption suggests it is similar to a mid B supergiant. The high luminosity, high mass loss rate, moderate wind velocity of 110 km s^{-1}, and presence of a circumstellar nebula all are hallmarks of an LBV. The massive dusty ring nebula surrounding G79* indicates a period of much higher mass loss in the recent past (Paper I), possibly during a red supergiant phase. The star may evolve into a Wolf-Rayet star. Variability has not been demonstrated, but given the paucity of observations this is not surprising. More detailed spectra, such as those recently obtained for the Pistol Star (Najarro et al. 1998) and FMM362 (Geballe et al. 2000), are needed for G79* in order to allow quantitative analysis, including a direct estimate of the mass loss rate, and more careful comparison with other LBVc's and LBV's.

Acknowledgements. We thank P.W. Morris for permission to reproduce the K band spectra of AG Car and Wra 751, M. van Kerkwijk for the spectrum of SGR 1806-20, and A. de Koter and B. Wolf for helpful comments. We also thank the $\dot{M}$ group in Utrecht for useful discussions. LBFMW acknowledges financial support from a NWO "Pionier" grant. F. N. acknowledges DGYCIT grants PB96-0883 and ESP98-1351 UKIRT is operated by the Joint Astronomy Centre on behalf of the U.K. Particle Physics and Astronomy Research Council. We have made use of the SIMBAD database, operated at the Centre de Données Astronomiques, Strasbourg, France.

References

Bernat A.P., Lambert D.L., 1978, PASP 90, 520
Bowen I.S., 1947, PASP 59, 196
Chiosi C., Maeder A., 1986, ARA&A 24, 329

Chlewicki G., van der Zwet G.P., van Ijzendoorn L.J., et al., 1986, ApJ 305, 455
Conti P.S., 1984, In: Meader A., Renzini A. (eds.) Observational test of Stellar evolution theory. IAU Symposium 105, p. 233
Fuchs Y., Mirabel F., Chaty S., et al., 1999, A&A 350, 891
Geballe T.R., Najarro F., Figer D.F., 2000, ApJ in press
Grandi S.A., 1975, ApJ 196, 465
Hamann F., Simon M., 1987, ApJ 327, 876
Higgs L.A., Wendker H.J., Landecker T.L., 1994, A&A 291, 295 (HWL)
Kurucz R.L., 1979, ApJS 40, 1
Lopes D.F., Damineli Neto A., de Freitas Pacheco J.A., 1992, A&A 261, 482
McGregor P.J., Hyland A.R., Hillier D.J., 1988, ApJ 324, 1071
Morris P.W., Eenens P.R.J., Hanson M.H., et al., 1996, ApJ 470, 597
Mountain C.M., Robertson D., Lee T.J., Wade R., 1990, Proc. SPIE 1235, 25
Münch G., 1948, ApJ 108, 116
Najarro F., Hillier D.J., Kudritzki R.P., et al., 1994, A&A 285, 573
Najarro F., Hillier D.J., Figer D.F., Geballe T.R., 1998, In: Falcke H., Cotera A., Huschl W., Melia F., Rieke M. (eds.) The Central Parsecs. Galactic Center Workshop 1998, in press
Nota A., Clampin M., 1997, In: Nota A., Lamers H. (eds.) Luminous Blue Variables: Massive stars in transition. ASP Conference Series vol. 120
Nota A., Lamers H. 1997, In: Nota A., Lamers H. (eds.) Luminous Blue Variables: Massive stars in
Odenwald S.F., Campbell M.F., Shivanandan K., et al., 1990, AJ 99, 288
Thompson R.I., Boroson T.A., 1977, ApJ 216, L75
Torres-Dodgen A.V., Tapia M., Carroll M., 1991, MNRAS 249, 1
Trams N.R., van Tuyll C.I., Voors R.H.M., et al., 1999, In: Wolf B., Fullerton A., Stahl O. (eds.) Variable and Non-spherical Stellar Winds in Luminous Hot Stars. IAU Colloquium 169
van Kerkwijk M.H., Kulkarni S.R., Matthews K., Neugebauer G., 1995, ApJ 444, L33
Voors R.H.M., 1999, Thesis, University of Utrecht
Waters L.B.F.M., Izumiura H., Zaal P., et al., 1996, A&A 313, 866 (Paper I)